J|A|C|S ARTICLES

Published on Web 05/10/2010

Bridged Photochromic Diarylethenes Investigated by Ultrafast Absorption Spectroscopy: Evidence for Two Distinct Photocyclization Pathways

Stéphane Aloïse,*,† Michel Sliwa,† Zuzanna Pawlowska,† Julien Réhault,†,|| Julien Dubois,† Olivier Poizat,† Guy Buntinx,† Aurélie Perrier,*,‡ François Maurel,‡ Shouhei Yamaguchi,§ and Michinori Takeshita§

Laboratoire de Spectrochimie Infrarouge et Raman (UMR 8516 du CNRS), Centre d'études et de recherches Lasers et Applications (FR 2416 du CNRS), Université des Sciences et Technologies de Lille, Bat C5, 59655 Villeneuve d'Ascq Cedex, France, Laboratoire Interfaces, Traitements, Organisation et Dynamique des Systèmes (ITODYS), CNRS UMR 7086, Université Paris 7 - Paris Diderot, Bâtiment Lavoisier, 15 rue Jean Antoine de Baif, 75205 Paris Cedex 13, France, and Department of Chemistry and Applied Chemistry, Faculty of Science and Engineering, Saga University, Honjo1, Saga 840-8502, Japan

Received December 22, 2009; E-mail: stephane.aloise@univ-lille1.fr; aurelie.perrier-pineau@univ-paris-diderot.fr

Abstract: Two photochromic diarylethenes blocked by alkyl bridges in an ideal conformation for photocyclization are studied by stationary and femtosecond transient spectroscopy in order to depict the photocyclization processes: the bistable 1,2-dicyano[2.*n*]metacyclophan-1-ene with $n = 2$, abbreviated as [2.2], and its non-bistable analogue with $n = 4$, abbreviated as [2.4]. The data are interpreted in the light of AM1-CIS calculations and state correlation diagrams based on conclusive TD-DFT calculations. For [2.2], a solvent-sensitive excitation wavelength threshold governing the photocyclization yield is clearly evidenced between the S_1 and S_2 singlet states. Excitation above and beyond this threshold induces two distinct photochemical pathways. The S_1 vertical excitation induces direct efficient ($\phi \approx 0.9-1$), and ultrafast ($\sim$120 fs) photocylization from S_1 open form that leads to a ground-state transition structure, probably through a conical intersection, then to a hot cyclized ground state that relaxes by vibrational cooling. Upon higher excitation energy, the system undergoes internal conversion to the hot S_1 state, then evolves toward the cyclized S_1 state and relaxes by ultrafast S_1-S_0 internal conversion. Alternatively, the possibility for a second conical intersection near hot S_1 state is discussed. This second photoclosure reaction is less efficient and both the photocylization yield and overall kinetics depend on solvent polarity ($\phi = 0.49$, $\tau = 2.5$ ps in nonpolar solvent; $\phi = 0.7$, $\tau = 1.5$ ps in polar solvent). In the case of [2.4], for which the distance between the two reactive carbons is larger, a unique photoclosure mechanism is found and a structural effect is reported. Indeed, this mechanim is similar to the above second reaction of [2.2] but characterized by much slower kinetics ranging from 12 to 20 ps (depending on the excitation wavelength and solvent polarity). All polarity effects are rationalized in terms of stabilization of the transient states of charge-transfer character involved in the photocyclization process.

1. Introduction

Photochromism is a photoinduced reversible transformation between two chemical forms having different absorption spectra.[1] This reaction is of great importance due to its actual implications for the development of photomemory and photoswitching materials.[1] Among all photochromic families, diarylethenes are some of the most efficient compounds used for photoswitching applications because of their thermal irreversibility, high fatigue resistance, and good photoconversion yield between an open form (OF) and a closed form (CF).[2a] For those reasons, numerous recent advances based on diarylethene photochemistry have been reported.[2b] However, the photocyclization (OF→CF) yield, a fundamental photochemical parameter for applications, is seriously limited in classical diarylethenes by the existence of two OF conformers having anti and syn configurations and among which only the former is photoactive.[1,2] An attractive approach to overcome this limitation is to lock the molecule in an ideal conformation by incorporating a rigid link. Recently, Takeshita et al. succeeded

† Université des Sciences et Technologies de Lille.
‡ Université Paris 7 - Paris Diderot.
§ Saga University.
|| Current address: Universität Zürich Physikalisch Chemisches Institut Winterthurerstrasse 190 CH-8057 Zürich.

(1) Bouas-Laurent, H.; Dürr, H. *Photochromism*; Elsevier Science B.V.: Amsterdam, 2003.

(2) (a) Irie, M. *Chem. Rev.* **2000**, *100*, 1685. (b) Tsuboi, Y.; Shimizu, R.; Shoji, T.; Kitamura, N. *J. Am. Chem. Soc.* **2009**, *131*, 12623. (c) Al-Atar, U.; Fernandes, R.; Johnsen, B.; Baillie, D.; Branda, N. R. *J. Am. Chem. Soc.* **2009**, *131*, 15966. (d) Morimoto, M.; Miyasaka, H.; Yamashita, M.; Irie, M. *J. Am. Chem. Soc.* **2009**, *131*, 9823. (e) Wing-Wah Yam, V.; Ka-Wai Lee, J.; Ko, C. C.; Nianyong, Z. *J. Am. Chem. Soc.* **2009**, *131*, 912.

Chart 1

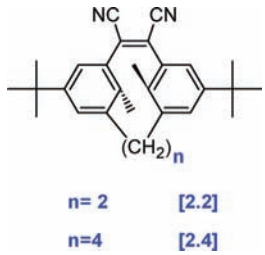

in performing such challenging synthesis of a series of metacyclophan-1-ene photochromic compounds in which the two reacting aryl groups are maintained in an antiparallel conformation by the presence of an additional alkyl bridge of variable length *n* (see Chart 1).[3]

Interest in these bridged compounds was stimulated by preliminary results.[3] First, it was shown that the thermal stability of the metacyclophan-1-ene CF can be varied by changing the length of the alkyl bridge.[3] Then, an improvement for the photocyclization yield was reached but not as significant as could be expected.[3] In order to understand the reason for this moderate improvement and the parameters controlling the photoswitching efficiency, we have undertaken a thorough investigation of the photochemical reactivity of representative bridged diarylethenes by ultrafast pump−probe spectroscopy and quantum chemical calculations.

In this paper, we focus our attention on two specific bridged photochromic compounds among those previously studied,[3] the 1,2-dicyano[2.*n*]metacyclophan-1-enes with alkyl chain lengths $n = 2$ and 4, abbreviated as [2.2] and [2.4], respectively (Chart 1): [2.2] is a bistable photochromic compound since the thermal back reaction is very slow (CF lifetime of the order of 50 days at 273 K).[3] A total recovery of the starting OF material can be readily achieved by visible light irradiation without any significant photodegradation.[3] As already mentioned, the improvement of the photocyclization yield has reached only a few percent: $\phi_{OF\rightarrow CF} = 0.39$ for [2.2] vs 0.35 for the unconstrained analogue (upon 313 nm excitation in nonpolar solvent).[3] In contrast, [2.4] is not stable in the CF and undergoes thermal back reaction to the OF so rapidly that the spectral characterization of the CF by stationary spectroscopy is not possible even at low temperature.[3] As a consequence, its photocyclization yield cannot not be determined.

Concerning the photochemistry of unconstrained diarylethenes, it has been established that the fundamental processes occur on a picosecond time scale, photoopening reaction (CF→OF) occurring in more than 10 ps and photocyclization in a faster 1 − 10 ps time domain, depending on the molecular structure.[4−10,13] Note that for this latter process, direct identification of CF precursor by transient spectroscopy has never been achieved due to the lack of isosbestic points related to its formation. Alternatively, theoretical investigations including CASSCF calculations have attempted to describe the overall photochemical pathway. These studies concluded, for model diarylethenes, the participation of S_0/S_1 conical intersections in the photocyclization process,[14−16] a result often generalized to most of the diarylethenes. However, recent experimental studies pointed out the fact that the knowledge of the S_1 photochemical pathway was not sufficient anymore to fully understand the photoreversion and photocyclization reactions of the diarylethene family. Indeed, investigating the ring-opening reactions, Miyasaka et al. demonstrated that the photoreversion yield can be enhanced through multiphoton absorption, which suggests that the photoconversion process could be more efficient in higher singlet states S_n than in the S_1 state via one-photon absorption.[17] However, such additional S_n photoactive pathways are not yet characterized. Fukaminato et al. recently performed photocyclization yield measurements as a function of the excitation wavelength and observed a threshold wavelength effect that they explain in terms of distinct singlet and triplet photoreactivity.[18] Additionally, Irie et al. discovered the possibility to tune the photochromic yields by changing the polarity of the solvent through charge-transfer (CT) excited-state conformations.[19]

By analogy with unbridged diarylethenes and with particular attention to the photoinduced ring-closure process in [2.2] and [2.4], we performed photocyclization yield measurements, subpicosecond time-resolved absorption experiments for various excitation wavelengths and for various solvents. We discovered important effects that might be of fundamental importance for the photochromism's community: (i) constraining the diarylethene with an alkyl bridge opens two distinct photochemical channels (Kasha's rule violations) that lead to the same colored form; (ii) the branching ratio between the two channels would be dependent on the solvent polarity; (iii) faster (few hundred

(3) (a) Takeshita, M.; Yamato, T. *Tetrahedron Lett.* **2001**, *42*, 4345. (b) Takeshita, M.; Inoue, M.; Hisasue, H.; Maekawa, S.; Nakamura, T. *J. Phys. Org. Chem.* **2007**, *20*, 830.
(4) Tamai, N.; Saika, T.; Shimidzu, T.; Irie, M. *J. Phys. Chem.* **1996**, *100*, 4689.
(5) Owrutsky, J. C.; Nelson, H. H.; Baronavski, A. P.; Kim, O. K.; Tsivgoulis, G. M.; Gilat, S. L.; Lehn, J.-M. *Chem. Phys. Lett.* **1998**, *293*, 555.
(6) (a) Hania, P. R.; Telesca, R.; Lucas, L. N.; Pugzlys, A.; Van Esch, J. H.; Feringa, B. L.; Snijders, J. G.; Duppen, K. *J. Phys. Chem. A* **2002**, *106*, 8498. (b) Hania, P. R.; Pugzlys, A.; Lucas, L. N.; De Jong, J. J. D.; Telesca, R.; Feringa, B. L.; Van Esch, J. H.; Duppen, K. *J. Phys. Chem. A* **2005**, *109*, 9437.
(7) (a) Miyasaka, H.; Nobuto, T.; Itaya, A.; Tamai, N.; Irie, M. *Chem. Phys. Lett.* **1997**, *269*, 281. (b) Miyasaka, H.; Nobuto, T.; Murakami, M.; Itaya, A.; Tamai, N.; Irie, M. *J. Phys. Chem. A* **2002**, *106*, 8096.
(8) Okabe, C.; Nakabayashi, T.; Nishi, N.; Fukaminato, T.; Kawai, T.; Irie, M.; Sekiya, H. *J. Phys. Chem. A* **2003**, *107*, 5384.
(9) Shim, S.; Eom, I.; Joo, T.; Kim, E.; Kim, K. S. *J. Phys. Chem. A* **2007**, *111*, 8096.
(10) Ern, J.; Bens, A. T.; Martin, H.-D.; Mukamel, S.; Schmid, D.; Tretiak, S.; Tsiper, E.; Kryschi, C. *J. Lumin.* **2000**, *87−89*, 742.
(11) (a) Ern, J.; Bens, A. T.; Bock, A.; Martin, H.-D.; Kryschi, C. *J. Lumin.* **1998**, *76−77*, 90. (b) Ern, J.; Bens, A. T.; Martin, H.-D.; Mukamel, S.; Schmid, D.; Tretiak, S.; Tsiper, E.; Kryschi, C. *Chem. Phys.* **1999**, *246*, 115.
(12) Shim, S.; Joo, T.; Bae, S. C.; Kim, K. S.; Kim, E. *J. Phys. Chem. A* **2003**, *107*, 8106.
(13) Bens, A. T.; Ern, J.; Kuldova, K.; Trommsdorff, H. P.; Kryschi, C. *J. Lumin.* **2001**, *94−95*, 51.
(14) Nakamura, S.; Irie, M. *J. Org. Chem.* **1988**, *53*, 6136.
(15) Boggio-Pasqua, M.; Ravaglia, M.; Bearpark, M. J.; Garavelli, M.; Robb, M. A. *J. Phys. Chem. A* **2003**, *107*, 11139.
(16) (a) Asano, Y.; Murakami, A.; Kobayashi, T.; Goldberg, A.; Guillaumont, D.; Yabushita, S.; Irie, M.; Nakamura, S. *J. Am. Chem. Soc.* **2004**, *126*, 12112. (b) Nakamura, S.; Kobayashi, T.; Takata, A.; Uchida, K.; Asano, Y.; Murakami, A.; Goldberg, A.; Guillaumont, D.; Yokojima, S.; Koatake, S.; Irie, M. *J. Phys. Org. Chem.* **2007**, *20*, 821. (c) Uchida, K.; Guillaumont, D.; Tsuchida, E.; Mochizuki, G.; Irie, M.; Murakami, A.; Nakamura, S. *THEOCHEM* **2002**, *579*, 115.
(17) (a) Miyasaka, H.; Murakami, M.; Itaya, A.; Guillaumont, D.; Nakamura, S.; Irie, M. *J. Am. Chem. Soc.* **2001**, *123*, 753. (b) Miyasaka, H.; Murakami, M.; Okada, T.; Nagata, Y.; Itaya, A.; Kobatake, S.; Nakamura, S.; Irie, M. *Chem. Phys. Lett.* **2003**, *371*, 40. (c) Ishibashi, Y.; Tani, K.; Miyasaka, H.; Kobatake, S.; Irie, M. *Chem. Phys. Lett.* **2007**, *437*, 243. (d) Tani, K.; Ishibashi, Y.; Miyasaka, H.; Kobatake, S.; Irie, M. *J. Phys. Chem. C* **2008**, *112*, 11150.
(18) Fukaminato, T.; Doi, T.; Tanaka, M.; Irie, M. *J. Phys. Chem. C* **2009**, *113*, 11623.
(19) Irie, M.; Sayo, K. *J. Phys. Chem.* **1992**, *96*, 7671.

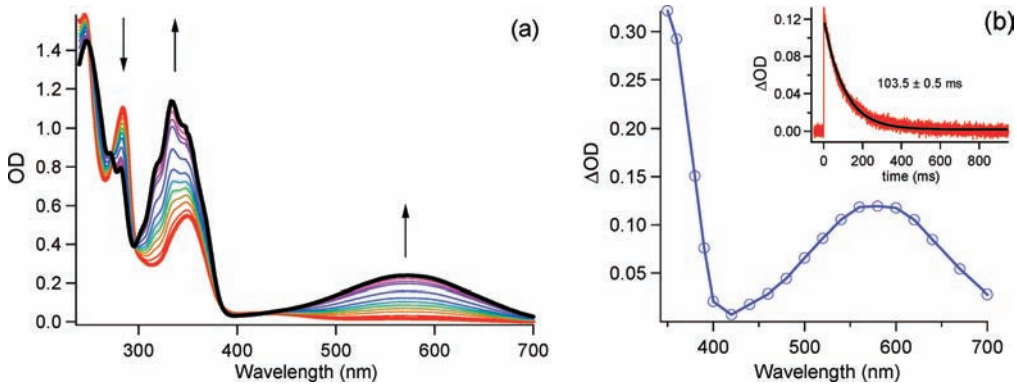

Figure 1. (a) Absorption spectra of [2.2] in acetonitrile under continuous UV irradiation acquired every 1 min; the arrows indicate the temporal evolution. (b) Transient absorption spectrum of [2.4] in acetonitrile (20 μs delay time) under 355 nm laser excitation. The inset shows the decay of the 595 nm absorption band.

femtoseconds) processes are found compared with unbridged diarylethenes; (iv) depending on the excitation wavelength and solvent polarity, the photocylization quantum yield can be optimized for appropriate conditions. In the following, we will demonstrate with the help of theoretical calculations that all these findings can be interpreted in terms of two distinct photochromic singlet pathways, and we believe that such results would be of extended importance for the general understanding of diarylethene molecules and related applications.

2. Experimental and Theoretical Methods

The syntheses of [2.2] and [2.4] are published elsewhere.[3] Typical sample concentrations used in time-resolved experiments were 5×10^{-4} M. The Sigma-Aldrich acetonitrile (ACN), hexane (HX), and ethanol (EtOH) solvents were used as received, and spectroscopic measurements were performed in pure ACN and mixed solvents (HX/EtOH 12:1).

2.1. Spectroscopic Measurements. Stationary absorption was recorded with a CARY-100B Bio absorption spectrometer. Two different experiments were performed for the bistable [2.2] molecule to evaluate its photocoloration yield (for [2.4] see below). First, the photocoloration yield ϕ(313 nm) was determined according to a standard procedure using the 313 nm line of a Mercury lamp and bis(2-methyl-1-benzothien-3-yl)hexafluorocyclopentene as reference molecule.[20] Additionally, the photocoloration yields at various wavelengths were performed using an ORIEL Xe lamp (1000 W) equipped with a monochromator. In order to correlate these measurements with previous ones, all data ϕ (λ) were normalized with respect to the 313 nm excitation wavelength measurement according to

$$\phi(\lambda) = \frac{I_0(313\text{ nm})}{I_0(\lambda)} \times \frac{1 - 10^{-A_{OF}(313\text{ nm})}}{1 - 10^{-A_{OF}(\lambda)}} \times \frac{(\dot{A}_{CF})_\lambda}{(\dot{A}_{CF})_{313\text{ nm}}} \phi(313\text{ nm}) \quad (1)$$

where I_0 denotes the incident light power, A_{OF} is the open form absorbance at irradiation wavelength λ, and $\dot{A}_{CF} = dA_{CF}/dt$ is determined by fitting with linear slope the time evolution of the closed form absorption maximum under continuous irradiation, i.e., $A_{CF} = f(t)$ (see Figure 1). Only the first 30 min was acquired in order to avoid exponential curvatures.

The nanosecond laser (Nd:YAG)-flash photolysis apparatus used for the determination of the [2.4] back-thermal reaction and photocoloration yields ratio has been described elsewhere.[22] The measurements consist of acquiring the kinetics of appearance of CF either for 266/355 nm excitations in a given solvent or for a given excitation in different solvents and then computing the intensity ratio after normalizing all data according to the benzophenone triplet reference signal.

The pump−probe subpicosecond absorption experiments were carried out using an amplified Ti:sapphire laser (BM Industries) delivering 0.8 mJ and 80 fs pulses tunable between 766 and 800 nm with a repetition rate of 1 kHz.[22] The 390 nm pump pulses were obtained by frequency doubling the fundamental at 780 nm, while the 266 nm pump pulses were obtained by frequency tripling the fundamental at 800 nm. About 3 mJ·cm^{-2} was provided by the pump in both cases. The probe beam was generated by focusing 1 μJ of the fundamental on a 1 mm CaF_2 plate giving a white light continuum with a spectrum covering the UV−vis and near IR range. The probe beam was split into signal and reference beams before crossing the sample, and the resulting beams were recorded on two different channels of a multichannel spectrograph equipped with a CCD camera. Transient absorbance was obtained by comparing signal and reference spectra for different time delays. The time delay between the pump and probe was varied up to 1.5 ns (using a micrometric optical delay line), and the temporal resolution of the apparatus was better than 300 fs. All of the transient traces presented in this paper are GVD corrected according to the typical extrapolation method.[21] Furthermore, the characteristic times deduced from kinetics are obtained by fitting the uncorrected data with the result of a multiexponential function convolved with a Gaussian pulse (which approximates the pump−probe correlation function) and taking into account GVD and OD due to thickness of the sample (see eq 16 of ref 21).[21] Pump and probe beams, with relative linear polarizations set at the magic angle, were focused in a 2 mm flow cell equipped with CaF_2 windows. Note that an additional Xe lamp with green filter is continuously lighting the sample reservoir for a maximum regeneration of the OF species after its conversion into the CF by the action of the laser pump excitation.

2.2. Theoretical Calculations. The spectral properties of [2.2] and [2.4] were simulated following a three-step methodology[23a] based on density functional theory (DFT) and time-dependent DFT (TD-DFT): (i) the ground-state geometry of each structure was optimized without symmetry constraints in the gas phase with DFT; (ii) the vibrational spectrum is computed at the same level of theory to confirm that the optimized structures correspond to true minima

(20) Uchida, K.; Tsuchida, E; Aoi, Y.; Nakamura, S.; Irie, M. *Chem. Lett.* **1999**, *28*, 63.

(21) (a) Nakayama, T.; Amijima, Y.; Ibuki, K.; Hamanoue, K. *Rev. Sci. Instrum.* **1997**, *68*, 4364. (b) Ziŏlek, M.; Lorenc, M.; Naskręcki, R. *Appl. Phys. B: Laser Opt.* **2001**, *72*, 843.

(22) Aloïse, S.; Réhault, J.; Moine, B.; Poizat, O.; Buntinx, G.; Lokshin, V.; Valès, M.; Samat, A. *J. Phys. Chem. A* **2007**, *111*, 1737.

(23) (a) Jacquemin, D.; Perpète, E. A.; Ciofini, I.; Adamo, C. *Acc. Chem. Res.* **2009**, *42*, 326. (b) Maurel, F.; Perrier, A.; Perpète, E. A.; Jacquemin, D. *J. Photochem. Photobiol. A* **2008**, *199*, 211.

on the potential energy surface; and (iii) the vertical transition energies to the excited states are computed with TD-DFT. All calculations were performed using the Gaussian 03 package.[24]

For steps i and ii, we have used the 6-311G(d) triple-ξ polarized basis set, while for step iii, the more extended 6-311+G(d) basis set has been used to obtain converged transition energies. For the geometry optimizations, we have used the PBE0 functional[25] that provides accurate ground-state structure for most organic systems and particularly for photochromic molecules.[23] For TD-DFT calculations, four hybrid functions with different percentages of exact exchange were tested: B3LYP (20% of exact exchange),[25a] PBE0 (25%),[25b] BMK (42%),[25c] and BHandHLYP (50%).[25d] For vertical transition energy calculations, solvent effects were introduced by using the polarizable continuum model (PCM).[26] Most of the theoretical results are reported in the Supporting Information. Table SI1 (Supporting Information) lists the wavelengths computed for the first transitions of [2.2] and [2.4] open-ring isomers with B3LYP, PBE0, BMK, and BHandHLYP functionals. These four functionals actually provide the same qualitative results. Quantitatively, if we focus on the intense $S_0 \rightarrow S_2$ transition, the excitation wavelength calculated with the BMK functional is in closer agreement with experimental results (absolute error of 0.13 eV for [2.2] and 0.03 eV for [2.4]). Consequently, in the following text we will stick to the PCM-TD-BMK/6-311+G(d)//PBE0/6-311G(d) calculation scheme.

To investigate the ring-closure/ring-opening mechanism, we should determine some characteristic properties of the ground state as well as the excited-state potential energy surfaces (PES). The description of the excited states PES at the ab initio level requires the use of a multiconfigurational self-consistent field (MC-SCF) method such as the complete active-space SCF (CASSCF) approach. Unfortunately, the correct description of the excited states of the considered molecule requires CASSCF calculations involving the distribution of 18 π electrons in 18 π orbitals (18e, 18o), which is not feasible at the present time for such a large system. Calculations with a reduced (14e, 14o) active space, excluding the cyano groups, have led to significant differences in the frontier orbitals delocalization and in the nature of the excited singlet states. This underlies the crucial role of CN substituents on the excited state properties of [2.2] and [2.4]. Alternatively, semiempirical calculations using configuration interaction (CI) have proven to be useful to obtain the approximate wave function and molecular geometry of the electronic excited states.[27] Therefore, the semiempirical configuration interaction using all possible single excitations (AM1-CIS) available in the AMPAC 8.0 package[28] was used for the optimization of the excited states. All singly excited configurations involving the nine highest occupied and nine lowest unoccupied orbitals, which correspond to the π and π^* orbitals, were included in the CIS expansion. The reliability of the AM1-CIS method has been extensively tested for conjugated molecules: this method was shown to reproduce qualitatively the geometry of ground and excited states.[29] For spectroscopic results, Tables SI1 and SI2 (Supporting Information) show that the vertical energy transitions of the low-lying excited states (S_1 and S_2) are in good agreement with TD-DFT calculations and experiments. For [2.2] (respectively [2.4]), TD-DFT calculations underestimate the $S_0 \rightarrow S_1$ transition by -0.19 eV (-0.05 eV), while CIS overestimates this transition by 0.31 eV (0.41 eV). For the $S_0 \rightarrow S_2$ excitation, TD-DFT provides a signed error of $+0.13$ eV for [2.2] (-0.03 eV for [2.4]), while CIS is in close agreement with experiment (-0.04 eV for [2.2] and 0.0 eV for [2.4]). In the latter case, the exceptional agreement between CIS and experimental features certainly partially originates in error cancellation. An inspection of the molecular orbitals has shown that excitations calculated at the CIS level imply the same orbitals as TD-DFT calculations. Nevertheless, the oscillator strengths calculated at the semiempirical level are in discrepancy with TD-DFT and experiments: the CIS $S_0 \rightarrow S_1$ transition is predicted to be more intense than the $S_0 \rightarrow S_2$ transition. For the higher energetic states (S_3 to S_5), comparison between CIS calculations and experimental features is no longer straightforward. AM1-CIS calculations will thus be used to investigate the geometries and energetic profiles of the S_1 and S_2 low-lying excited states, and particular precaution will be taken concerning the predicted oscillator strength.

Table 1. Spectrokinetic Properties and Photochromic Quantum Yields (Absolute and Relative Values) for [2.2] and [2.4] in ACN and HX/EtOH (12:1)

		λ_{max} (nm)		ϕ(OF→CF)			
		OF	CF	$\lambda = 313$ nm	$\lambda > 400$ nm	ratio ϕ	τ_Δ (ms)
[2.2]	HX/CH_2Cl_2 9:1	340[a]	555[a]	0.39[a]			
	HX/EtOH 12:1	345	560	0.49	0.9	0.71−0.90[b]	
	ACN	350	575	0.69	1		
[2.4]	HX/EtOH 12:1	330	575			0.93[c]	62.5
	ACN	335	595				103.5

[a] Reference 3. [b] Ratio = ϕ(HX/EtOH 12:1)/ϕ(ACN), computed from absolute values. [c] From laser flash photolysis measurement at 355 nm excitation.

Scheme 1

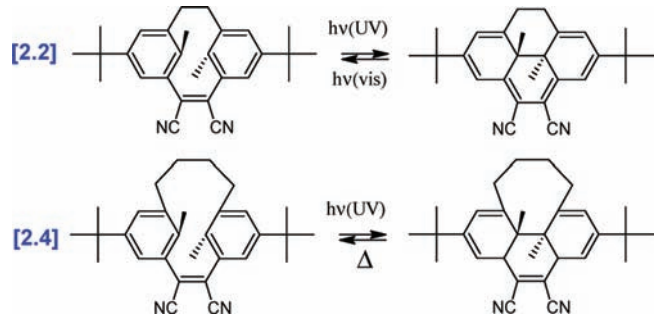

3. Results

3.1. OF and CF Spectrokinetic Characterizations. Upon UV irradiation, a colorless solution of [2.2] in either acetonitrile or HX/EtOH (12:1) becomes rapidly purple. All spectrokinetic data are tabulated for both solvents in Table 1. For the ACN case, Figure 1a shows the evolution of the UV−vis absorption spectra of [2.2] under continuous broad band UV excitation during 15 min.

The initial spectrum, recorded before irradiation, shows a band at 350 nm typical of the uncolored OF. Then a gradual evolution is seen with irradiation time: this modification is characterized by two isosbestic points at 274 and 297 nm and is related to the photochromic photocyclization (Scheme 1) between OF and CF, the latter species being well recognized with the new visible absorption band maximizing at 570 nm (note also a sharp UV band with vibrational structure peaking at 325, 335, and 345

(24) *Gaussian 03, Revision C.02*. Frisch, M. J. et al. Gaussian, Inc., Wallingford, CT, 2004.
(25) (a) Becke, A. D. *J. Chem. Phys.* **1993**, *98*, 5648. (b) Adamo, C.; Barone, V. *J. Chem. Phys.* **1999**, *110*, 6158. (c) Boese, A. D.; Martin, J. M. L. *J. Chem. Phys.* **2004**, *121*, 3405. (d) Becke, A. D. *J. Chem. Phys.* **1993**, *98*, 1372.
(26) Tomasi, J.; Mennucci, B.; Cammi, R. *Chem. Rev.* **2005**, *105*, 2999.
(27) Maurel, F.; Aubard, J.; Millie, P.; Dognon, J. P.; Rajzmann, M.; Guglielmetti, R.; Samat, A. *J. Phys. Chem. A* **2006**, *110*, 4759.
(28) AMPAC 8, 1992−2004 Semichem, Inc., PO Box 1649, Shawnee, KS 66222.
(29) (a) Agmon, N.; Rettig, W.; Groth, C. *J. Am. Chem. Soc.* **2002**, *124*, 1089. (b) Gedeck, P.; Schneider, S. *J. Photochem. Photobiol. A: Chem* **1999**, *121*, 7. (c) Lambert, C.; Risko, C.; Coropceanu, V.; Schelter, J.; Amthor, S.; Gruhn, N.; Durivage, J.; Bredas, J. L. *J. Am. Chem. Soc.* **2005**, *127*, 8508.

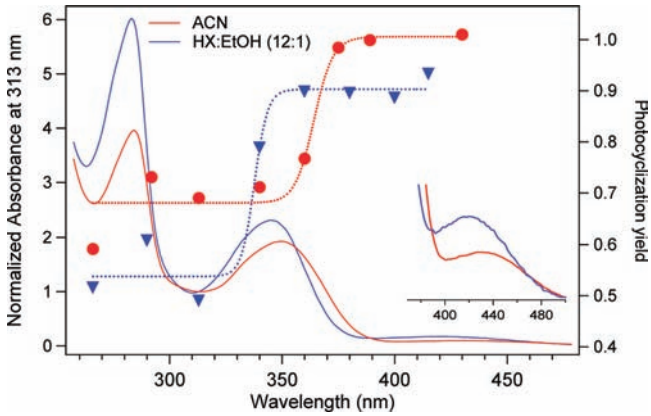

Figure 2. Photocoloration quantum yields of [2.2] for different excitation wavelengths in ACN and (HX/EtOH 12:1). The absorption spectrum of [2.2] is also included (inset: spectra × 20). The sigmoid functions (dashed lines) are purely illustrative.

nm). In the less polar solvent, a moderate hypsochromic effect is noticed for both OF and CF (see Table 1). Additionally, a hyperchromic effect is observed for OF (see Figure 2) but not for CF (not shown).

In the case of [2.4], it was not possible to follow the time evolution of the absorption spectrum by the above procedure due to too fast thermal back-reaction, and nanosecond flash photolysis measurements were performed consequently. Figure 1b shows the presence of a photoinduced broad transient visible absorption band peaking at ca. 595 nm in ACN that can be likely ascribed to the CF of [2.4] by analogy with the 570 nm stationary absorption band of [2.2]. In HX/EtOH (12:1), a similar hypsochromic effect is observed for OF and CF, as seen in Table 1, while in regard to the intensity spectra, a hyperchromic effect is also obtained for OF but not CF. A solvent polarity effect is found also for the lifetime of [2.4] CF at ambient temperature, which decreases from 103.5 ms in ACN to 62.5 ms in HX/EtOH (12:1).

3.2. Wavelength- and Polarity-Dependent Photocoloration Yields. Because CT character appears preeminent from stationary data, new photocoloration yield measurements upon 313 nm excitation were achieved for [2.2] in both ACN and HX/EtOH (12:1). As shown in Table 1, the new photocoloration yield increases with the solvent polarity from 0.49 in HX/EtOH (12:1) to 0.69 in ACN. To gain more information on the fundamental photochromic processes, the photocoloration yield measurements were extended to different excitation wavelengths between 266 and 430 nm in both solvents (Figure 2). Striking effects are clearly detected. Indeed, in ACN, the photocoloration yield suddenly raises from a value of about 0.7 in the UV region to a value of 1 at excitation wavelengths longer than a threshold value around 360 nm. In the less polar solvent, this threshold wavelength is lowered (around 330 nm) and the photocoloration yield variation is larger, increasing from 0.5 below the threshold to 0.9 beyond it. Note that those effects are nicely parallel to the hyperchromic trend found for OF.

Trying to study in more detail the excitation wavelength dependency in [2.4] was tricky due to the nonaccordability of our laser source. Measurements at 355 and 266 nm excitation, using benzophenone as actinometer, allowed us to assess a ratio $\phi(355)/\phi(266) = 0.93$, indicating that, unlike [2.2], no significant excitation wavelength effect characterizes [2.4]. To investigate the solvent effect, time-resolved measurements were realized in HX/EtOH (12:1) and ACN. A photocoloration yield ratio of

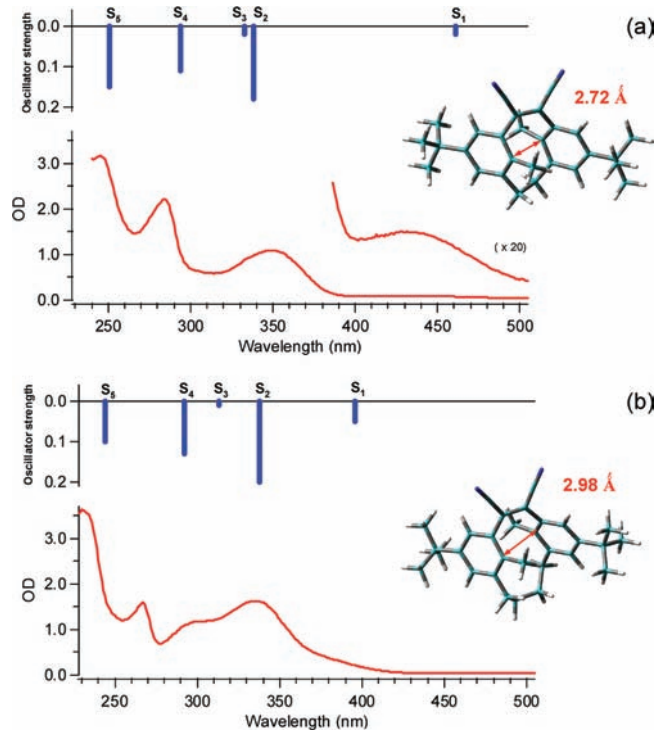

Figure 3. Absorption spectra of the open form of [2.2] (a) and [2.4] (b) in acetonitrile (red curve) together with TD-DFT excitation energies and oscillator strength (bold blue sticks). Theoretical DFT geometries are included indicating the increasing distance between the two reactive carbons (r_{cc}).

0.94 was determined, pointing out some lack of solvent polarity influence on the photocyclization process in [2.4].

3.3. OF and CF Theoretical Characterizations. From a structural point of view, the OF-optimized DFT geometries, included in Figure 3, underline the notable difference for the distance between the two reactive carbons in the ground state: 2.72 Å for [2.2] vs 2.98 Å for [2.4]. One can also notice that, from [2.2] to [2.4], the torsion between the two sides of the molecule (see Table SI3, Supporting Information) increases, leading to a conjugation loss. In contrast, no such differences are found for the CF geometries (see Table SI3, Supporting Information) with both reactive carbon distances close to 1.57 Å. Consequently, comparing the photophysics of the two molecules (see below), structural effects are mostly expected for the OF species.

The TD-DFT-computed wavelengths and oscillator strengths for [2.2] and [2.4] open forms in acetonitrile are compared to experimental spectra as shown in Figure 3 (see also Table SI1 (Supporting Information), where electronic transition attributions are also given). The noticeable agreement between experiments and calculations enables us to attribute with confidence the [2.2] and [2.4] absorption spectra to transitions from the S_1 up to the S_5 singlet excited state.

Influence of Alkyl Bridge Length on OF Absorption Spectra. On going from [2.2] to [2.4], a hypsochromic shift (−40 nm in ACN) is observed for the $S_0 \rightarrow S_1$ transition while the $S_0 \rightarrow S_2$ and $S_0 \rightarrow S_3$ bands, which cannot be distinguished for [2.2], are separated for [2.4] with a wavelength difference of 38 nm in ACN. These two structural effects can be explained by an inspection of the molecular orbitals involved in the electronic excitations. Indeed, in [2.2] and [2.4], the OF first excited state, S_1^{FC}(OF), corresponds to a charge transfer (CT)

Chart 2. HOMO and LUMO Orbitals (BMK/6-311G(d), Contour Threshold of 0.03 au)

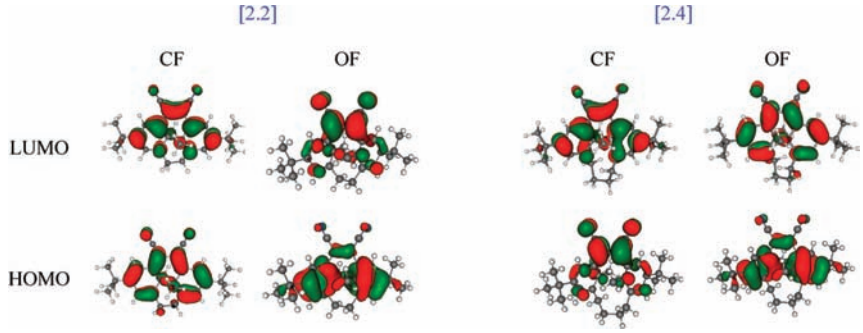

from the HOMO, essentially localized on the central double bond, to the LUMO, rather involving the cyano substituents. The latter can be assumed to be quite insensitive to alkyl bridge modifications, while the HOMO shows an antibonding character between the two reactive carbons and will thus be stabilized by a longer distance. As a consequence, from [2.2] to [2.4], the HOMO stabilization combined with the LUMO insensitivity leads to an increase of the HOMO−LUMO gap and thus to a hypsochromic effect for the HOMO→LUMO transition. Additionally, the strong structural effect found for the $S_0 \rightarrow S_3$ (HOMO-2→LUMO) transition energy is likely rationalized by observing the HOMO-2 orbital (see Table SI4, Supporting Information). For [2.2], this orbital presents a strong and unexpected contribution of the σ alkyl bridge orbital which leads to an antibonding interaction between the σ and π systems. For [2,4], the larger distance between the two reactive carbons lessens this antibonding interaction and stabilizes the HOMO-2 orbital. Therefore, the σ/π coupling yields an increase of the HOMO-2/LUMO gap, the corresponding electronic transition is tuned toward smaller wavelength, and the S_2-S_3 states are split up.

Solvent Polarity Effects on OF and CF Absorption Spectra. The hypsochromic solvent effect that shifts the OF absorption bands with increasing solvent polarity (Figure 2) can be well predicted by TD-DFT calculations (Table SI1, Supporting Information). For instance, for the S_0 (HOMO)→S_1 (LUMO) transition of [2.2] ([2.4]), calculations foresee a hypsochromic shift of −26 nm (−20 nm) in agreement with the −10 nm (−10 nm) displacement experimentally observed. This effect results from the stabilization of the LUMO by polar solvents, which thus reduces the HOMO−LUMO gap. The same conclusion holds for the S_2 state which corresponds, for both [2.2] and [2.4], to an electron promotion from the HOMO-1, centered on the photochromic core, to the LUMO. The hyperchomic effect on intensity is likely related with the strong CT character for the OF as indicated on Table 3.

For both CF molecules (Table SI2, Supporting Information), the visible band can be assigned to the S_0 (HOMO)→S_1 π,π^* (LUMO) transition while the UV band near 350 nm is ascribed to the S_0 (HOMO)→S_3 (LUMO+1) transition. These frontier orbitals are delocalized on the photochromic unit with small contributions of the cyano groups, accounting for the moderate solvatochromic effect experimentally observed.

3.4. Subpicosecond Transient Absorption Measurements at Different Excitation Wavelengths. To better understand the photocyclization process, time-resolved experiments were performed both below and beyond the characteristic threshold of [2.2], using 266 and 390 nm excitations. For comparison, similar transient measurements were performed for [2.4]. According to the assignment of the absorption spectra established above (Figure 3b), the 266 and 390 nm excitations are respectively expected to populate up to the S_5 and S_1 excited states (S_2 state foot band as well) in the case of [2.2], up to the S_4 and S_1 excited states in the case of [2.4].

[2.4] OF Excited at 266 and 390 nm. For [2.4] in acetonitrile, transient absorption spectra recorded in the 300−670 nm spectral range within time windows of 0.5−1.1 and 1.4−400 ps following 266 nm excitation are shown in parts a and b, respectively, of Figure 4. Similar measurements following 390 nm excitation (for 400−750 nm spectral range) are shown in parts c and d of Figure 4. The description of these transient spectra is straightforward and can be done globally for both excitation cases. At early times (Figure 4a,c) a broad signal covering the entire spectral range increases and evolves toward a more structured spectrum with three well-defined bands peaking at 350 nm (band A), 470 nm (band B), and 700 nm (band C). The growth times are identical for the three bands and equal to 190 ± 50 fs and 480 ± 80 fs for 390 and 266 nm excitation, respectively (see Table 2). At longer times (Figure 4b,d), these bands decay concomitantly with a similar time constant of ∼20 ps (see Table 2), leading to a final spectrum showing two bands at 360 and 595 nm, stable on the 100−1500 ps time range. This last spectrum is readily ascribable to the ground-state CF of compound [2.4] as it is undeniably similar to the spectrum observed for this species in the flash photolysis experiment (Figure 1b). Strictly similar spectra were obtained in HX/EtOH (12:1) (see Table 2), the characteristic times of bands A/B/C displaying, however, lower values. Some excitation wavelength dependency of these times is also noticed. For example, on going from ACN to HX/EtOH (12:1), the decay time of bands A/B/C decreases from ∼20 to ∼16 ps at 390 nm excitation and from ∼17 to ∼12 ps at 266 nm excitation.

[2.2] OF Excited at 266 nm. For [2.2] in acetonitrile, transient absorption spectra following 266 nm excitation, recorded in the 300−670 nm spectral range, within time windows of 0.6−1.2 and 1.4−200 ps, are shown in parts a and b, respectively, of Figure 5. A clear analogy is observed between these spectra and those previously discussed for [2.4] (Figure 4a,c). At short times, the transient spectrum includes two absorption bands peaking at about 480 and 635 nm analogous to band B and band C of [2.4] and a highly structured spectral frame with positive and negative sharp peaks in the 300−370 nm region (rather than the unique band A seen for [2.4]). All features appear first with a characteristic time of 400 ± 40 fs (see Table 2). The decay of these bands involves two exponential contributions. In the 450−700 nm region, bands B and C decay with a single exponential time constant 1.5 ± 0.1 ps. At the end of this decay, a broad band maximizing around 560 nm is apparent and keeps constant intensity at longer times. This band is unambiguously ascribed to the ground-state CF species by

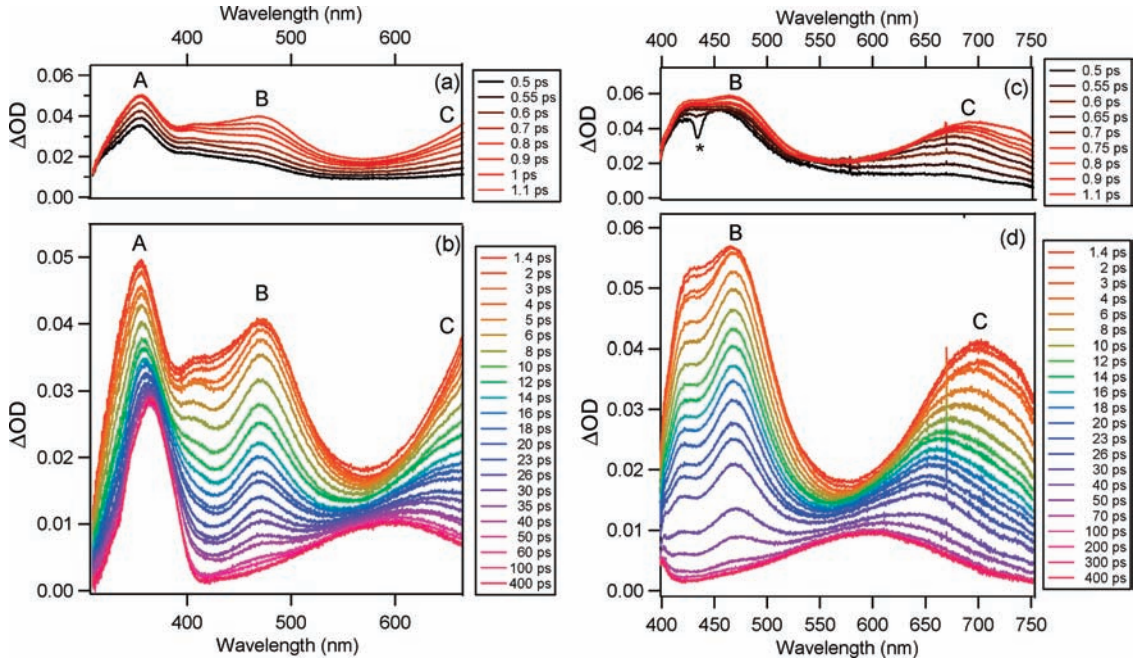

Figure 4. Subpicosecond time-resolved absorption spectra of [2.4] in acetonitrile using 266 nm (left) and 390 nm (right) excitation wavelengths within the 0.5−1.1 ps (a, c) and 1.4−400 ps (b, d) temporal windows. All spectra are corrected from the GVD. The star indicates stimulated Raman peak.

Table 2. Characteristic Times for [2.2] and [2.4] in ACN and (HX/EtOH 12:1) Obtained from the Best Fits of the Subpicosecond Time-Resolved Absorption Kinetics Measured at Appropriate Wavelengths

			growth A/B/C (ps)	decay A/B/C (ps)	growth D (ps)	decay D (ps)
[2.2]	390 nm	HX/EtOH 12:1			<0.1	0.11 (2)
		ACN			<0.1	0.12 (4)
	266 nm	HX/EtOH 12:1	0.25 (4)	2.5 (1)[a]		
		ACN	0.40 (4)	1.5 (1)[a]		
[2.4]	390 nm	HX/EtOH 12:1	0.13 (2)	16.4 (7)		
		ACN	0.19 (5)	20.5 (2)		
	266 nm	HX/EtOH 12:1	0.34 (4)	11.5 (5)		
		ACN	0.48 (8)	17 (1)		

[a] Only bands B and C.

analogy with the steady-state spectrum (Figure 1a). On the basis of the structural effect on the ring-closure reaction (predicted in section 3.3), it is tempting to propose that the CF of [2.2] is thus formed with a time constant of 1.5 ps, while this process requires 20 ps for [2.4]. Besides the temporal evolution of bands B and C, the 380 nm absorption band decays biexponentially (time constants 1.5 and 13 ps) concomitantly with the disappearance of the 300−370 nm sharp structure and the growth of a new absorption band peaking at 335 nm (an isosbestic point is seen at 355 nm). The remaining 335 nm band corresponds, as does the 560 nm feature, to the ground state CF species. If the 1.5 ps decay is already assigned, the 13 ps contribution reveals the presence of an additional photoinduced process. The band structure observed in the 300−370 nm region shows two sharp minima at 330 and 350 nm that correspond approximately to the position of the vibronic maxima in the UV absorption band of CF (see the black curve in Figure 1a). It reveals the probable presence of some bleaching of the CF ground state of [2.2] superimposed on the transient absorption band. Such a bleaching contribution can be explained by the high stability of both forms for [2.2] and consequently the presence of some amount of steady-state CF during the measurement. As a confirmation, the CF bleaching contribution was found to notably increase for long acquisition periods, i.e., after long irradiation times. We thus propose that the 13 ps dynamic processes corresponds to the overall excited-state decay of CF including the $S_1 \rightarrow S_0$ deactivation and photoreversion processes. Similar data have been obtained in HX/EtOH (12:1) except for an exponential time of 2.5 ps for the decay of bands A/B/C (see Table 2).

[2.2] OF Excited at 390 nm. In ACN, spectra recorded in the 400−750 nm spectral range within time windows of 0.3−0.5 and 0.525−10 ps following 390 nm excitation are presented in parts c and d, respectively, of Figure 5. In contrast to the similarity of the spectral evolution observed for [2.4] upon photolysis at 390 and 266 nm, a clear excitation wavelength effect is seen for [2.2]. At short times (Figure 5c), a broad band covering the entire 400−750 nm region undergoes a notable red-shift from about 450 nm at 300 fs to 700 nm at 650 fs. This ultrafast band shift, clearly apparent in the contour plot representation of Figure 6b, is completed at 650 fs and has a characteristic time evaluated to be less than 100 fs (see Table 2). The 650 fs trace is representative of a transient band noted band D in the following. A simultaneous decay of band D is observed up to 1.2 ps and leads to a final spectrum characterized by a broad absorption maximizing at 570 nm typical of the ground state CF but with broader width. The final CF spectrum (see Figure 1a) is finally recovered within about 10 ps via a process that can be safely attributed to vibrational relaxation of the colored form (we will not try to fit this last process because of its minor spectral contribution). The global fitting analysis of the ultrafast band D decay, performed using the deconvolution approach of Ziolek et al. (see, for example, the 500 and 690 nm traces in Figure 6a) leads to a characteristic time of 120 ± 40 fs. As a consequence, we provide clear spectroscopic evidence for the existence of two different ring closure dynamics. Similar data were obtained in HX/EtOH (12:1) (see Table 2).

[2.2] CF Excited at 390 nm. In order to investigate the CF excited-state dynamics, we performed similar time-resolved

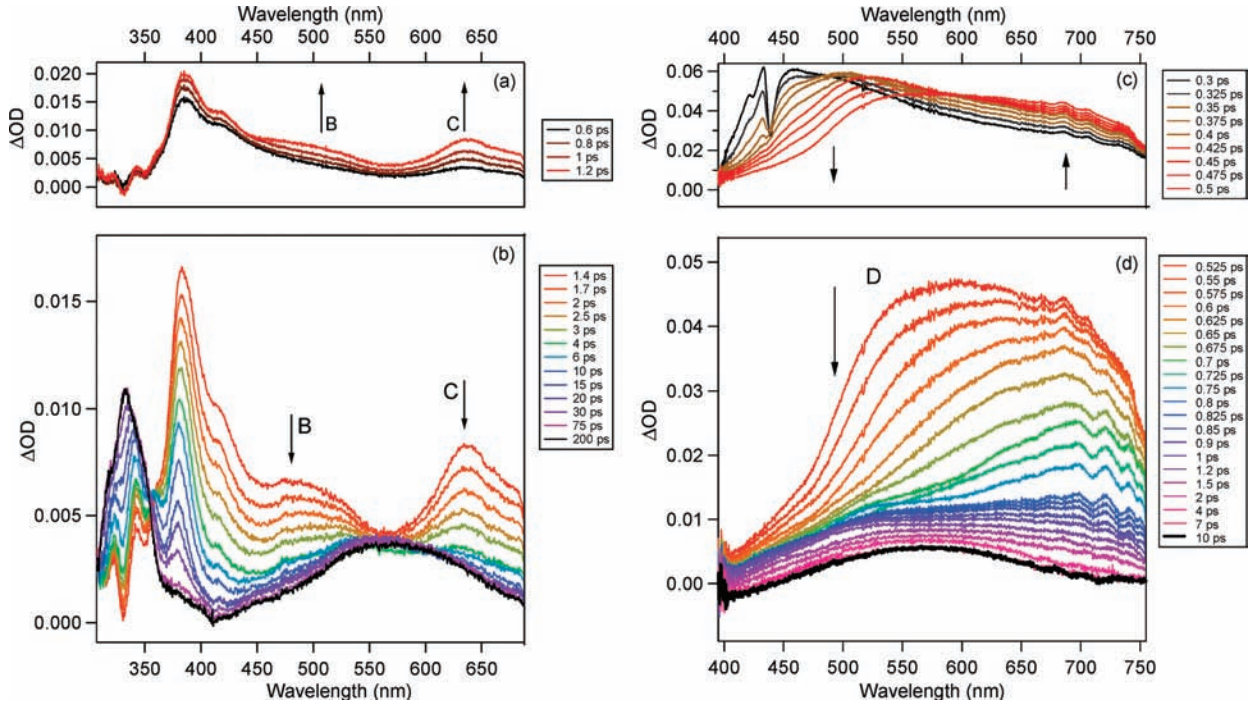

Figure 5. Subpicosecond time-resolved absorption spectra of [2.2] in acetonitrile using 266 nm (left) and 390 nm (right) excitation wavelengths. The temporal windows are different: 0.6−1.2 ps (a) and 1.4−200 ps (b); 0.3−0.5 ps (c) and 0.525−10 ps (d). All spectra are corrected from the GVD. The sharp peak in part c is due to stimulated Raman diffusion.

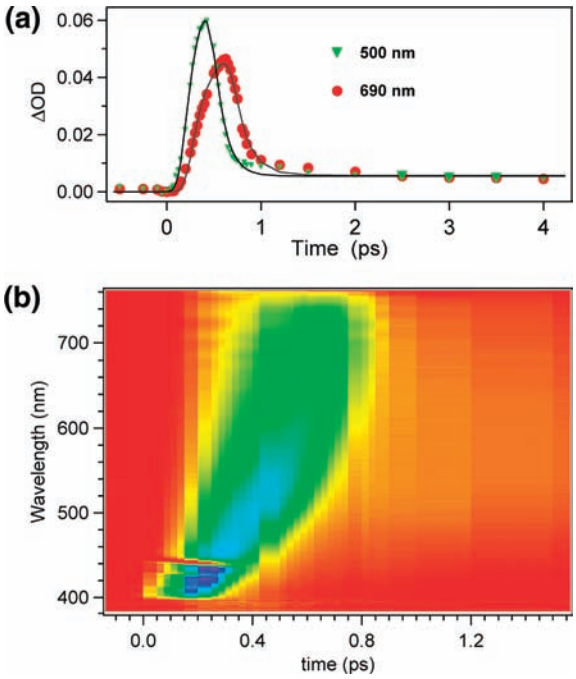

Figure 6. (a) 500 and 690 nm kinetic traces obtained for molecule [2.2] with 390 nm and best fits to exponentials evolutions (see the Experimental and Theoretical Methods for more details); (b) contour plot obtained from Figure 5 and expanded between 0 and 1.4 ps.

experiments on a [2.2] purple solution (photostationary state achieved after 30 min UV irradiation) with a CF proportion estimated to be higher than OF proportion (results shown in Figure SI2a, Supporting Information). According to Table SI2 (Supporting Information), the 390 nm excitation populates the S_1 state of CF. Within the 0.3−0.9 ps time window, an initial broad negative signal is likely assigned to CF bleaching superimposed to some OF* excited state absorption (probably band D) resulting from the direct excitation of the OF population present in the initial sample in addition to CF. The decay of this broad signal gives rise to the hot CF, S_0(CF, v*), spectrum, which decays via vibrational relaxation during the 1−20 ps time window (Figure SI2b, Supporting Information). The characteristic times for these two processes are 250 fs and 2.5 ps, respectively. Considering the nonnegligible contribution of OF*, it appears difficult to assign precisely those times. However, they provide upper estimations of the characteristic times related to the S_1(CF)→S_0(CF, v*) internal conversion, i.e., 250 fs, and vibrational relaxation of S_0(CF, v*), i.e., 2.5 ps.

3.5. Ground and Excited Potential Energy Surfaces. For [2.2] and [2.4], the first (S_1 and S_2) singlet excited-state potential energy surfaces (PES) calculated at the AM1-CIS level are shown in Figure 7. The reaction coordinate is represented by the distance between the two reactive carbons r_{cc} as shown in Figure 3. For [2.2], the geometry of the S_0(CF) and S_0(OF) isomers has been optimized at the AM1-CIS level leading to a trifling difference with TD-DFT-optimized structures (see Table SI3, Supporting Information). The S_0(CF)−S_0(OF) energy path, obtained by using the CHAIN method,[30] shows the existence of a transition state S_0(TS) with a r_{cc} distance of 1.99 Å and a barrier of activation for ring closure of 1.67 eV (39 kcal·mol^{-1}). S_0(TS) geometrical parameters are closer to the S_0(CF) geometry than to the S_0(OF) structure. For the first excited state, from the Franck−Condon geometry S_1^{FC}(OF), the system relaxes to its minimum energy structure S_1(OF). The value of the reaction coordinate is considerably shortened on going from S_1^{FC}(OF) (r_{cc} = 2.70 Å) to S_1(OF) (r_{cc} = 2.18 Å). On the ring-closure reaction path, the system then reaches a transition state S_1(TS) for a r_{cc} distance of 1.94 Å. The energy barrier to ring closure on the S_1 PES is very small 0.03 eV (0.7 kcal·mol^{-1}). After

(30) (a) Liotard, D. A.; Penot, J. P. *Numerical Methods in the Study of Critical Phenomena*; Springler-Verlag: Berlin, 1981; p 213. (b) Liotard, D. A. *Int. J. Quantum Chem.* **1992**, *44*, 723.

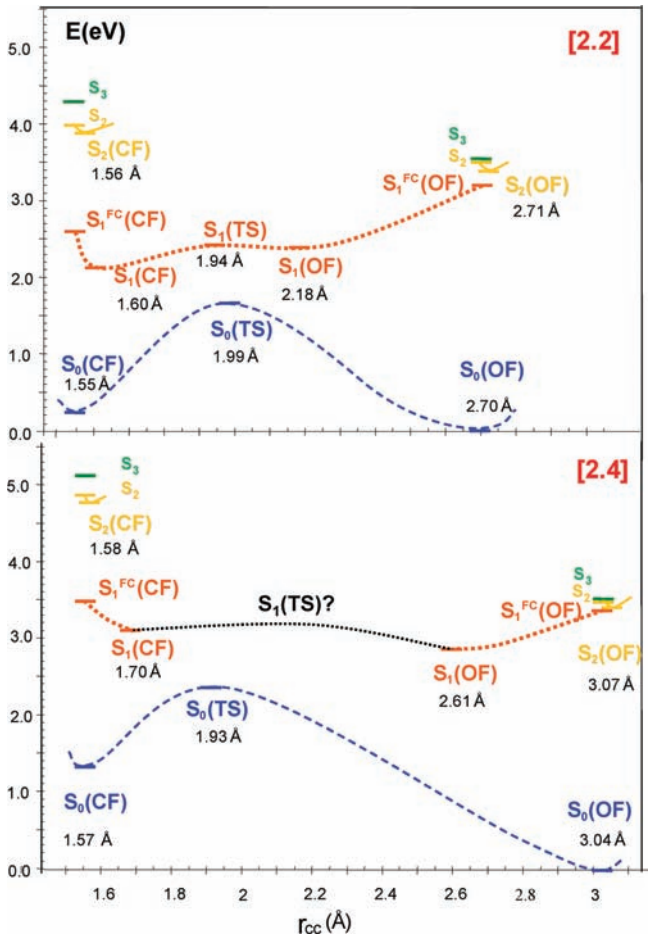

Figure 7. Ground- and first excited-state potential energy surfaces of [2.2] and [2.4] calculated at the AM1-CIS level. For both systems, the reference energy corresponds to S_0(OF).

reaching this transition state, a decrease in the potential energy leads to the closed-ring region of the PES and to the S_1(CF) minimum. This critical point (r_{cc} = 1.60 Å) is close to the S_1^{FC}(CF) geometry (r_{cc} = 1.55 Å). It is worth noting that the geometries of the different critical points on the PES are close to C_2 symmetry (Table SI3, Supporting Information). For the S_2 state, following the gradient in the Franck−Condon region leads to the S_2(OF) minimum with r_{cc} slightly stretched on going from S_2^{FC} (OF) (2.70 Å) to S_2(OF) (2.71 Å). Unfortunately, since AM1-CIS vertical excitations for the S_3, S_4, S_5 states did not provide satisfying comparisons with experiment and TD-DFT, we could not investigate the PES of these excited states.

To investigate the structural effect observed in section 3.3, we then compare the ground-state and excited-state PES of [2.2] and [2.4]. For the ground state, the transition state S_0(TS) of [2.4] is still localized in the closed-ring region as it was the case for [2.2] (Figure 7), and the energy barrier for ring-closure on the S_0 PES (2.62 eV, i.e., ~60.5 kcal·mol^{-1}) is much higher than the barrier for [2.2]. The optimization of the S_1(OF) structure from the FC region shortens the r_{cc} distance compared with the S_1(OF) structure of [2.2]. This indicates that the first intermediate on the S_1 PES of [2.4] is alike the OF geometry in contrast with [2.2]. The transition state search on the S_1 PES failed, which suggests that the PES is rather flat between S_1(OF) and S_1(CF). The dotted black line in Figure 7 is an illustration of this hypothesis.

State Correlation Diagrams. Since the AM1-CIS calculations could not provide information concerning the more energetic S_n potential energy surfaces and could not locate topological features (conical intersections, etc.), we have built the state correlation diagrams between OF and CF (Figure 8) for both [2.2] and [2.4]. These qualitative diagrams have been drawn according to usual procedure and assuming a C_2 symmetry (asymmetric and symmetric correlation lines are displayed in blue and black, respectively).[31] In the past, such diagrams have been successfully used by Irie et al. for the rationalization of thermal irreversibility[16] or the cycloreversion quantum yield.[7] Concerning the state energies, we took advantage of the TD-DFT results which are in good agreement with experiments (see Table SI1 (Supporting Information) and Figure 3) in order to derive state correlation diagrams. Note that the molecular orbitals (MO) used to build this correlation diagram[31] are displayed in Table SI3 (Supporting Information). Two main effects have to be commented for those diagrams. First, one recognizes the well-known S_0/S_n avoided crossing (hereafter CI_1) with adiabatic curves joining OF(S_0) and CF(S_0) states. This is consistent with known diarylethene photochemistry in which ultrafast dynamics is a result of such conical intersection.[14−18] However, unexpected correlation lines within the asymmetric manifold are found for the bridged diarylethene. Indeed, rather than the well-known correlation between the S_0 and S_1 states of OF and CF (due to HOMO→LUMO correlation) encountered for standards diarylethenes,[32] the CF S_1 state is correlated with the OF S_5 state (HOMO→LUMO+1 excitation) and S_8 state (HOMO→LUMO+3 excitation) in the case of [2.2] and [2.4] respectively. More details on these correlations are reported in the Supporting Information. As a consequence, two avoided crossings, named CI_2 and CI_3, arise after taking into account S_1-S_n(OF) and S_2-S_n(OF) asymmetric correlation lines.

4. Discussion

The spectrokinetic properties of the two bridged 1,2-dicyano[2,*n*]metacyclophan-1-enes studied in this paper display strong dependence on with solvent polarity conferred by the two acceptor cyano groups. The inspection of the molecular orbitals described in section 3.3 provides a straightforward rationalization of these main effects, underlining the charge-transfer character of the low-lying excited states of [2.2] and [2.4]. Furthermore, two separate results have demonstrated the existence of two distinct photocyclization pathways in the case of [2.2]: (i) a strong dependence of the photocoloration yield on the excitation wavelength is observed with a significant increase at a threshold wavelength lying between the $S_0\rightarrow S_1$ and $S_0\rightarrow S_2$ transitions, identified by TD-DFT (the wavelength threshold and the magnitude of the yield increase are both dependent on solvent polarity); (ii) the transient signal of [2.2] is totally different for an excitation below or beyond this threshold. Indeed, the complex and ultrafast 120 fs photocyclization dynamics arising upon 390 nm excitation ($S_0\rightarrow S_1$ transition), related to the observation of the transient absorption band D, is totally different from the 1.5 ps dynamics observed upon 266 nm excitation ($S_0\rightarrow S_n$ transition), related to the transient bands A/B/C. The latter transient absorption bands are also found to be involved in the photoreactivity of [2.4], which

(31) Rauk, A. *Orbital Interaction Theory of Organic Chemistry*; John Wiley & Sons, Inc.: New York, 2001.
(32) Perrier, A.; Maurel, F.; Aubard, J. *J. Photochem. Photobiol. A* **2007**, *189*, 167.

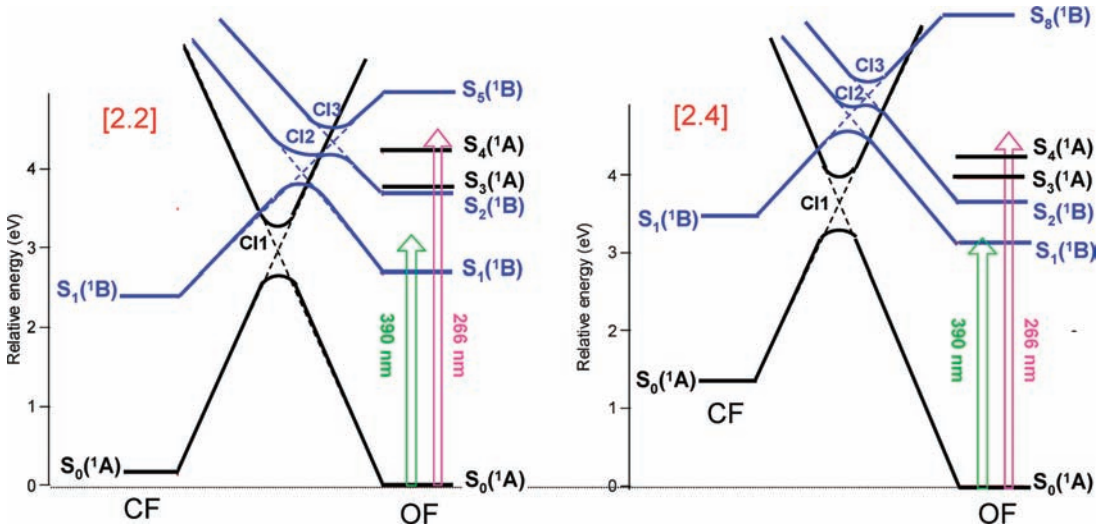

Figure 8. State correlation diagrams for [2.2] and [2.4] using TD-DFT vertical excitation energies where the OF ground-state level is taken as the reference energy. Black lines refer to symmetric states and blue lines for antisymmetric states (some correlation lines are not included for sake of simplicity). Laser excitations at 390 nm (green arrow) and 266 nm (pink arrow) are shown.

appears only moderately dependent on the excitation wavelength as well as the solvent polarity, and is characterized by time constants of ~12−20 ps that are much longer than those measured for [2.2]. This comparison gives evidence for a photocyclization process notably dependent on the reactive carbon interdistance. We will now focus on the identification of these two distinct photocyclization pathways with the help of AM1-CIS calculations (Figure 7) and correlation diagrams (Figure 8).

4.1. Two Distinct Photochemical Pathways. Let us consider first the reaction channel available within S_1 state excitation (390 nm excitation case), which is efficient for [2.2] (ϕ(355 nm)/ϕ(266 nm) > 1.4) but does not seem to be efficient for [2.4] (ϕ(355 nm)/ϕ(266 nm) = 0.93). The early cyclization dynamics, characterized by a substantial and ultrafast spectral shift occurring within less than 100 fs (Figure 5c) can be assigned to an electronic relaxation from the Franck−Condon S_1^{FC} states to the S_1(OF) along the S_1 potential surface as indicated in Figure 7. Note that the spectral shift may be likely correlated with the drastic geometric change calculated along the ring closure coordinate (Δr_{cc} = 0.52 Å) during this ultrafast electronic relaxation. At this stage, the extremely fast 120 fs decay of S_1(OF) (Band D) can be understood by i) the strikingly similar geometries of S_1(OF) (2.18 Å) and S_0(TS) (1.99 Å); ii) the avoided crossing CI_1 on the state correlation diagram linking the ground and excited PES. In summary, the ultrafast photoclosure reaction is expected to occur through a conical intersection, noticed CI_1, between S_1(OF) and S_0(TS), allowing efficient production of hot ground-state CF, {S_0,(CF),v*}. Finally, in accordance with experimental observations, fast vibrational relaxation is the final step in the photocyclization reaction. The whole photocyclization pathway can be cast, assuming an adiabatic transition from a totally relaxed singlet state S_1(OF), in the following way

$$S_0(OF) \rightarrow S_1^{FC}(OF) \rightarrow S_1(OF) \rightarrow (CI_1) \rightarrow \{S_0,(CF),v^*\} \rightarrow S_0(CF) \quad (2)$$

As further validation of this mechanism, relevant similarities have been found with the results of Hania et al. that report a 900 fs time closure through a conical intersection.[6b] Their conclusion was based on transient data exhibiting a strong spectral shift. The excellent photocylization yield measured for excitation above the energy threshold (near unity) is consistent with the striking proximity for the S_1(OF) minimum and transition state S_0(TS) predicted from AM1/CIS calculations (see Figure 7). Similarly, one can foresee in the case of [2.4] that the inefficiency of this mechanism is due to drastic geometrical differences between those two decisive topological features (Δr = 0.68 Å, see Figure 7). It seems more reasonable that, once the system has reached S_1(OF), it finds an appropriate funnel to relax toward the starting OF ground state.

Complete identification of the second photocyclization process and its solvent dependency is more challenging due to the need to rationalize two seemingly opposite results: on one hand, a similar photoreactive mechanism, different from the S_1 photochemical pathway, occurs for both molecules (similar spectral bands A/B/C); on the other hand, violation of Kasha's rules is observed only in the case of [2.2]. As a first hypothesis for solving this dilemma, S_2 state photoreactivity can be ruled out at first glance. Indeed, the AM1-CIS geometry of S_2 denotes an additional expansion of the molecule rather than an evolution in the ring closure direction. As a matter of fact, because the abrupt threshold for the photocyclization yield of [2.2] is lying between the S_1 and S_2 states, it seems reasonable to envisage the second photoreactive channel as originating from a topological region of the S_1(OF) potential curve located at higher energy compared to the S_1(OF) potential minimum. In this sense, AM1-CIS calculation predict the existence of a transition state S_1(TS) accessible only from a vibrationally excited S_1 state, abbreviated {S_1,(OF),v*}. We thus propose that the transient bands A/B/C arise, for both molecules, from this hot state. Within this hypothesis, the precyclization dynamics can be suggested to result from a fast population of the {S_1(OF),v*}from the initially excited Franck−Condon region by internal conversion, with a dynamics obeying the energy gap law as seen in Table 2 for the A/B/C bands growth time (the higher the excitation, the slower the internal conversion). Identification of the following step in the ring closure dynamics has to take into account the structural effect reported in section 3.4, i.e., a monoexponential A/B/C bands decay of 1.5−2.5 ps and 12−20 ps for [2.2] and [2.4], respectively. Inspection of AM1-CIS results indicates that

only OF excited species could be responsible for such effect rather than CF excited species (see below). Furthermore, no other intermediate is detected as precursor of CF, and it seems unlikely that photo-ring closure could occur neither directly from $\{S_1(OF),v^*\}$ nor through the conical intersection CI_1 discussed above. We suggest therefore the possible population of $S_1(CF)$ through $S_1(TS)$ followed by an ultrafast internal conversion (probably few hundreds of femtosecond) leading to $S_0(CF)$. As a confirmation, we assessed internal conversion of $S_1(CF)$ to be less than 250 fs (see Figure SI2 in the Supporting Information); this is also consistent with the 300 fs characteristic time reported by Ern et al.[11b] As a consequence, because one cannot distinguish such fast process compared to picosecond processes, the direct detectable precursor of CF (responsible for transient bands A/B/C) would be $\{S_1(OF),v^*\}$ rather than $S_1(CF)$. Summarizing the above propositions and assuming a light excitation to excited singlet state $S_n(OF)$, the second photocyclization pathway can be cast in the following form:

$$S_0(OF) \rightarrow S_n(OF) \rightarrow \{S_1(OF),v^*\} \rightarrow S_1(TS) \rightarrow S_1(CF) \rightarrow S_0(CF) \quad (3)$$

The structural effect reported in this study has to be rationalized by eq 3 and AM1-CIS results. Regarding the final electrocyclization process, it is worthwhile to corroborate the increasing decays from [2.2] (1.5−2,5 ps) to [2.4] (12−20 ps) to the drastic increasing distances between the reactive carbons in $S_1(OF)$, i.e. 2.18 Å and 2.61 Å respectively. (Obviously, one considers that hot S_1 state would has similar geometry compared to $S_1(OF)$.) Additionally, faster photoclosure process found for [2.2] can be likely related to the negligible 0.7 kcal.mol^{-1} potential barrier to overpass to go from $\{S_1(OF),v^*\}$ to $S_1(CF)$ (see $S_1(TS)$). In this sense, the longer photoclosure process for [2.4] can be related with the substantial endothermicity predicted between $S_1(OF)$ and $S_1(CF)$. Finally, note that the 1.5/2.5 ps closure time found for [2.2] is consistent with the 1−10 ps time set published by other groups for more conventional unbridged diarylethenes.[4,10−13]

Because no clear isosbestic point involving CF visible band has been reported in our transient spectra, it is still possible to find alternative mechanism for eq 3. In this sense, even if theoretical computations of advanced topological keypoints are not feasible in our case, correlation diagrams of Figure 8 predict unusual avoided crossing due to unusual S_1-S_5 or S_1-S_8 correlation lines. From the low energy avoided crossing (see CI_2 on figure 8) due to antisymmetric manifold, one can predict the existence of a conical intersection, abbreviated CI_2 as well, that would be responsible for direct CF production without any CF* species involved. It would allow rewriting eq 3 as

$$S_0(OF) \rightarrow S_n(OF) \rightarrow \{S_1(OF),v^*\} \rightarrow CI_2 \rightarrow S_0(CF) \quad (4)$$

Within this hypothesis, the energy position of CI_2 would be logically sensitive to solvent polarity. Final distinction between eq 3 and eq 4 could be achieved with the aid of CASSCF calculations for model bridged diarylethenes.

4.2. Rationalization of Solvent Effects on Transient Data. Further validation of eq 3 can be attempted by examining the solvent effect on the femtosecond data of [2.2] and [2.4] in light of the theoretical results (such an approach is impossible for eq 4 without precise conical intersection calculations). For [2.2] after 266 nm excitation, as seen in Table 2, the lifetime of the assumed precursor of CF decreases from 2.5 to 1.5 ps while the absolute CF yield increases from 0.49 to 0.69 on going from HX/EtOH (12:1) to ACN. To account for these solvent effects, the relative CT character of the low-lying excited states has been evaluated by analyzing the percentage of electronic delocalization of the LUMO on the cyano groups (excitation of the S_1 and S_2 states corresponds to an electron promotion toward the LUMO). As indicated in Table 3, it is tempting to invoke a stronger polar stabilization for $S_1(TS)$ state compared to $S_1(CF)$, since these two states present respectively 9% and 4% electron density on the CN groups. Assuming that diabatic transition occurs through any high vibrational level, this polar stabilization is assumed to reduce the potential barrier to overcome and consequently to lower the CF precursor lifetime and enhance the photocyclization yield. Reversely, the characteristic time (Table 2) increases with polarity for [2.4] (from ∼12−16 ps to ∼17−20 ps) while the photocyclization yield (Table 1) is not really affected by polarity changes. Even if $S_1(TS)$ is still unknown, the strong CT character of $S_1(OF)$ (12% LUMO electron density on the CN groups) is expected to induce polar stabilization and thus greater endothermicity compared to $S_1(CF)$, which should increase the lifetime of the CF precursor. Similarly, one notes in Table 2 that the lifetime of the precursor of CF depends on the excitation wavelength. The reported lower lifetimes for more energetic excitation are totally consistent with a diabatic transition depending on the excess of electronic energy.

Table 3. Description of the LUMO at the AM1-CIS Level: Percentage of the Electronic Density of the LUMO Localized on the Cyano Groups Alone and on the Cyano Groups Plus the Adjacent Carbon Atoms

	cyano groups (%)		cyano groups + adjacent carbons (%)	
	[2.2]	[2.4]	[2.2]	[2.4]
$S_0(OF)$	16	17	69	72
$S_1^{FC}(OF)$	16	17	69	47
$S_1(OF)$	9	12	47	58
$S_1(TS)$	7		36	
$S_1(CF)$	4	4	20	20
$S_0(TS)$	6	7	33	34
$S_0(CF)$	5	5	23	23

4.3. Optimizing the Photocyclization Yield? To the best of our knowledge, this study is the first one reporting two distinct photochemical pathways within the singlet manifold accounting for the same photocyclization transformation in diarylethenes. From an application point of view, the enhancement of the photocyclization yield of [2.2] from 0.39 (nonpolar solvent, UV excitation) to almost unity (polar solvent, near-visible excitation) is of fundamental importance. Indeed, we finally demonstrate the ability of the bridging alkyl chain to effectively increase the photochromic yield, providing, however, that a photoexcitation beyond the threshold is used. Thus, one can conclude that the functionality expected for the alkyl bridge, i.e., blocking the molecule in a unique photoactive antiparallel conformation, is fully validated. Unfortunately, the addition of such alkyl bridge induces serious electronic changes and opens a less efficient photochromic channel (eq 3 or 4) for excitation just above the more effective one (eq 1), leading finally to a decrease of the photocyclization yield upon UV excitation.

From a structural point of view, it is interesting to remark that the threshold on Figure 2, delimiting the branching ratio between mechanisms (2) and (3) (or (4)) depends on the charge-transfer character of the molecule (electronic delocalization toward cyano groups) through the $S_1(TS)$ (or CI_2) energy level. Additionally, it has been demonstrated that, if the alkyl chain

length influences the S_1 state energy level, a similar influence is logically expected for the CI_1 energy level as well. For too long alkyl chains, as is the case for [2.4], the more efficient mechanism (2) is totally quenched by the less efficient mechanism (3)/(4). New diarylethenes with novel bridges and ethylene substituents that maximize the photocyclization process through mechanism (2) for UV excitation should be a relevant approach to optimize bridged diarylethene.

5. Conclusions

Compared to standard diarylethenes, the lack of improvement found in previous studies[3] for the photocyclization yield of 1,2-dicyano[2.*n*]metacyclophan-1-ene diarylethenes with additional alkyl bridges locked in a favorable conformation has been rationalized in terms of two different photocyclization pathways. The two channels have been evidenced by femtosecond transient absorption spectroscopy and rationalized with the aid of state correlation diagrams and AM1-CIS calculations. Indeed, we demonstrate that changing the alkyl bridge length induces drastic changes within the OF and CF electronic states distribution allowing two different photocyclization pathways to be followed by the system. The first photocyclization pathway (eq 2) concerns mostly [2.2] and involves efficient $\phi \approx 1$ and ultrafast (120 fs) adiabatic transition through S_0/S_n conical intersection leading to hot S_0(CF) followed by vibrational relaxation. The unexpected second photocyclization pathway, displaying less efficiency and solvent dependent quantum yield ranging from ~0.4 to 0.7, can be explained through the reactivity of hot singlet state, $\{S_1$,(OF),v*$\}$. From this state, two possibilities are proposed: (i) a diabatic transition to S_1(CF) through a transition state S_1(TS) and followed by ultrafast internal conversion (eq 3) and (ii) an adiabatic transition through some conical intersection CI_2 leading to CF (eq 4). Polarity-dependent photocyclization quantum yields are explained in terms of some charge transfer character of either S_1(TS) or CI_2. Since the novel photophysical schemes found in this study have been related with structural features, alkyl chain length and charge transfer character, bridged diarylethene are good candidates to achieve a complete photocyclization yield optimization, i.e., $\phi = 1$ under UV excitation. In this sense, trying to generalize the two different photochemical paths evidenced in this study by investigating new bridged diarylethenes as well as some smaller model compounds allowing CASSCF theoretical calculations are now under investigation in our laboratories.

Acknowledgment. Part of this work is supported by a Grant-in-Aid for Science Research in a Priority Area New Frontiers in Photochromism (471) (No. 21021021) from the Ministry of Education, Culture, Sports, Science and Technology (MEXT), Japan, and a Grant-in-Aid for Scientific Research (C) (No. 21550119) from Japan Society for the Promotion of Science (JSPS), to whom M.T. feels grateful. We thank also the Groupement de Recherche PHENICS GDRI 93 from CNRS for its help in the development of this work.

Supporting Information Available: Table SI1: absorption spectra of [2.2] and [2.4] OF isomers computed with different functionals and with AM1-CIS. Table SI2: TD-DFT and AM1-CIS absorption spectra of [2.2] and [2.4] CF isomers. Table SI3: selected geometrical parameters of [2.2] and [2.4] CF and OF obtained from geometry optimization. Table SI4: relevant molecular orbitals. Figure SI1: Geometrical coordinate definitions. Figure SI2: Transient absorption spectra recorded for a photostationary mixture of CF and OF species. Additional description of the state correlation diagram. Full ref 24. This information is available free of charge via the Internet at http://pubs.acs.org/.

JA910813X